A thermal EHL investigation for size effect of finite line contact on bush-pin hinge pairs in industrial chains

Mingyu Zhang
College of Mechanical Engineering, Donghua University, Shanghai, China and School of Mechanical and Automotive Engineering, Qingdao University of Technology, Qingdao, China
Jing Wang
College of Mechanical Engineering, Donghua University, Shanghai, China
Peiran Yang
School of Mechanical and Automotive Engineering, Qingdao University of Technology, Qingdao, China, and
Zhaohua Shang, Yi Liu and Longjie Dai
Qingdao Choho Industrial Co., Ltd, Qingdao, China

Abstract

Purpose – This paper aims to study the influence of the dimension change of bush-pin on the pressure, oil film thickness, temperature rise and traction coefficient in contact zone by using a thermal elastohydrodynamic lubrication (EHL) model for finite line contact. Concretely, the effects of the equivalent curvature radius of the bush and the pin, and the length of the bush are investigated.

Design/methodology/approach – In this paper, the contact between the bush and pin is simplified as finite line contact. The lubrication state is studied by numerical simulation using steady-state line contact thermal EHL. A constitutive equation Ree–Eyring fluid is used in the calculations.

Findings – It is found that by selecting an optimal equivalent radius of curvature and prolonging the bush length can improve the lubrication state effectively.

Originality/value – Under specific working conditions, there exists an optimal equivalent radius to maximize the minimum oil film thickness in the contact zone. The increase of generatrix length will weaken the stress concentration effect in the rounded corner area at both ends of the bush, which can improve the wear resistance of chain.

Peer review – The peer review history for this article is available at: https://publons.com/publon/10.1108/ILT-10-2019-0448.

Keywords EHL, Finite line contact, Chain drive, Equivalent radius of curvature

Paper type Research paper

1. Introduction

Roller chains are composed of rollers, pins, bushes, inner and outer chain plates, as shown in Figure 1; bush chains do not contain rollers. Chains and sprockets will suffer from severe impacts when meshing under harsh working conditions, such as high speed and heavy load, resulting in serious problems such as lubrication failure, pin wear, noise and so on. For bush chain and roller chain, wear mainly happens between the bush and the pin pairs. From low to middle speed chain drives, the pin is damaged more easily. In the working process of the chain, the bush and the pin constitute a reciprocating swing hinge pair. The lubrication behavior, friction and wear mechanism are different from that of gear teeth or rolling element bearings. Up to now, the majority of researches concern more on wear by doing different kinds of wear experiments. Meng *et al.* (2000) studied wear characteristics of timing chain and found that the infiltrated layer and core structure of pin and bush parts are important factors, affecting the wear characteristics of chain. Xu *et al.* (2017) studied the wear-resisting performance of timing bush chain and found that the performance of seamed bush is better than that of seamless bush. Peeken and Coenen (1986) studied the effect of different lubrication conditions on the wear of chain drive hinges and considered the effects of

The current issue and full text archive of this journal is available on Emerald Insight at: **https://www.emerald.com/insight/0036-8792.htm**

Industrial Lubrication and Tribology
72/5 (2020) 695–701
Emerald Publishing Limited [ISSN 0036-8792]
[DOI 10.1108/ILT-10-2019-0448]

This study is supported by National Natural Science Foundation of China through Grant No. 51875298 and Natural Science Foundation of Shandong Province No. ZR2019MEE040.

Received 28 October 2019
Revised 18 November 2019
Accepted 18 November 2019

Figure 1 Precision roller chain

lubricant viscosity and anti-wear additives. Cheng *et al.* (2016) have done a series of work on the silent chain system, which provided a sound theoretical basis for the design of the silent chain.

Once the wear resistance of sleeve-pin hinge pair is improved, the service life of the chain will be increased, and the loss caused by the shutdown of mechanical equipment due to the replacement of the chain will be reduced. If welled lubricated, the contact between the bush and the pin is an EHL state. Otherwise a mixed lubrication or boundary lubrication may be formed. The work on chain drives from the viewpoint of lubrication has been very few, demonstrating the situation that the lubrication problem of chain drives has long been neglected. Rosenkranz *et al.* (2017) experimentally explored the influence for the laser textured surface pattern on the traction coefficient and wear under condition of low speed and light load on a ball-disk test rig. In this year, the authors (Zhang *et al.*, 2019) published their numerical results by the effect of chain number using an infinite line thermal EHL contact. Because the contact between the bush and the pin shaft is a line and the length of the bush is often short, the model of finite line contact should be used to simulate the problem. At present, the research of finite line contact has been used to focus on rolling element bearings. Ren *et al.* (2009) proposed a hybrid lubrication model of finite length line contact. Subsequently, Zhu *et al.* (2012) studied the finite length EHL problem considering the real geometry and surface roughness and gave the full-scale dynamic calculation. They pointed out that the end modification of finite length line contact pair was particularly important because of the existence of rough peaks. Mihailidis *et al.* (2013) solved the end-modified finite length EHL problem under heavy load condition by using a multi-grid method. The non-Newtonian fluid, thermal effect and oil starvation effect were considered comprehensively. Liu *et al.* (2012) studied size effect on the behavior of thermal EHL of roller pairs. But unlike rolling element bearings, the equivalent curvature radius of the contact area of sleeve-pin hinge pair, which increases with the increase of chain number, can be quite large.

In this paper, the bush-pin friction pair of the short pitch transmission precision roller chain has been studied by using a thermal EHL model for the finite line contact, and the thermal EHL of the contact zone is analyzed through various pressure distribution, oil film shape, temperature rise and friction coefficient.

2. Mathematical models and algorithms

2.1 Mathematical models

The calculation in this paper is carried out for short pitch transmission precision roller chains (International Standard ISO 606, 1994). As is shown in Figure 2, the contact between

Figure 2 Schematic diagram of the bush-pin

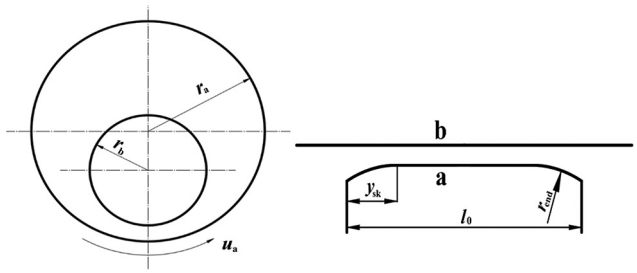

the bush and the pin is a conformal contact, a is bush, b is pin, and r_a and r_b are respectively the interior radius of the bush and the pin shaft. The speed of bush is u_a and the speed of pin is u_b. l_0 is the generatrix length of the bush, y_{sk} is the length of the rounded corner area at both ends of the bush, and r_{end} is the radius of the rounded corner.

The equivalent curvature radius r of the bush and the pin is calculated as:

$$r = r_a r_b / (r_a - r_b) \tag{1}$$

According to equation (1), the equivalent radii of curvature for chains No. 05B ~ 24B are calculated as shown in Table I. For the chain No. 05B, r = 54.516 mm, but for the chain No. 20 A, r = 2.28006 m. The variation range is very large, so that the size effect should be significant. The corresponding values of l_0, i.e. the generatrix lengths of bushes are also used in Table I, and big differences are found. The data for chain number greater than 24 A is not given in Table I because in fact, that large equivalent curvature radius brings forward divergence of calculations.

The constitutive equation of Ree-Eyring fluid (Yang, 1998) is employed:

$$\frac{\partial u}{\partial z} = \frac{\tau_0}{\eta} \sinh\left(\frac{\tau}{\tau_0}\right) \tag{2}$$

In equation (2), τ_0 is the characteristic shear stress of Ree–Eyring fluid, and η is the apparent viscosity of Ree–Eyring fluid.

The reciprocating swing motion between the bush and pin is simplified as a steady-state problem as a first step. Therefore, the Reynolds equation (Xu, 2011) used in the calculation is written as:

Table I Chain number, equivalent radius and bush length

No.	r (mm)	l_0(mm)	No.	r (mm)	l_0(mm)
05B	54.516	4.77	12A	891.200	17.75
06B	109.224	8.53	12B	330.044	15.62
08A	398.000	11.18	16A	1580.060	22.61
08B	200.000	11.3	16B	689.700	25.45
081	135.786	5.8	20A	2280.060	27.46
083	169.326	7.9	20B	1043.456	29.01
085	129.954	9.07	24A	2062.760	35.46
10A	434.350	13.84	24B	2147.684	37.92
10B	260.604	13.28			

$$\frac{\partial}{\partial x}\left[\left(\frac{\rho}{\eta}\right)_e h^3\frac{\partial p}{\partial x}\right]+\frac{\partial}{\partial y}\left[\left(\frac{\rho}{\eta}\right)_e h^3\frac{\partial p}{\partial y}\right]=12u_0\frac{\partial(\rho^* h)}{\partial x} \quad (3)$$

Because the radius of the rounded corner at both ends of the bush is very large, the linear speed on the inner surface of the bush is assumed to be the same. Thus in equation (3):

$$u_0=\frac{u_a+u_b}{2}$$

$$\left(\frac{\rho}{\eta}\right)_e=12\left(\eta_e\rho_e'/\eta_e'-\rho_e''\right)$$

$$\rho^*=\left[\rho_e'\eta_e(u_b-u_a)+\rho_e u_a\right]/u_0$$

The variables appearing in the above two formulas are defined as:

$$\rho_e=\frac{1}{h}\int_0^h\rho\mathrm{d}z$$

$$\rho_e'=\frac{1}{h^2}\int_0^h\rho\int_0^z\frac{\mathrm{d}z'}{\eta^*}\mathrm{d}z$$

$$\rho_e''=\frac{1}{h^3}\int_0^h\rho\int_0^z\frac{z'\mathrm{d}z'}{\eta^*}\mathrm{d}z$$

$$\frac{1}{\eta_e}=\frac{1}{h}\int_0^h\frac{\mathrm{d}z}{\eta^*}$$

$$\frac{1}{\eta_e'}=\frac{1}{h^2}\int_0^h\frac{z\mathrm{d}z}{\eta^*}$$

The boundary conditions of equation (3) is:

$$\begin{cases}p(x_{\mathrm{in}},y)=p(x_{\mathrm{out}},y)=p(x,-l)=p(x,l)=0\\ p\geq 0\ \ (x_{\mathrm{in}}<x<x_{\mathrm{out}},-l<y<l)\end{cases} \quad (4)$$

The film thickness equation (Xu, 2011) is:

$$h(x)=h_{00}+\frac{x^2}{2r}+h_{\mathrm{end}}+\frac{2}{\pi E'}\iint_\Omega\frac{p(x',y')}{\sqrt{(x-x')^2+(y-y')^2}}\mathrm{d}x'\mathrm{d}y' \quad (5)$$

where h_{00} is an unknown variable corresponding to the load w; h_{end} is the oil film thickness at the rounded corner area. The last item in the formula is the elastic deformation term, and E' is the equivalent elastic modulus between the two surfaces. The expression of h_{end} is:

$$h_{\mathrm{end}}=\begin{cases}\dfrac{(y+y_{\mathrm{sk}}-l)^2}{r_{\mathrm{end}}} & (-l\leq y<y_{\mathrm{sk}}-l)\\ 0 & (y_{\mathrm{sk}}-l\leq y\leq l-y_{\mathrm{sk}})\\ \dfrac{(y-y_{\mathrm{sk}}+l)^2}{r_{\mathrm{end}}} & (l-y_{\mathrm{sk}}<y\leq l)\end{cases} \quad (6)$$

In equation (6), $l=l_0/2$.

For a steady-state finite line contact, the energy equation of the lubricant film (Yang, 1998) is given as:

$$c\left(\rho u\frac{\partial t}{\partial x}+\rho v\frac{\partial t}{\partial y}-q\frac{\partial t}{\partial z}\right)-k\frac{\partial^2 t}{\partial z^2}$$

$$=-\frac{t}{\rho}\cdot\frac{\partial\rho}{\partial t}\left(u\frac{\partial p}{\partial x}+v\frac{\partial p}{\partial y}\right)+\eta^*\left[\left(\frac{\partial u}{\partial z}\right)^2+\left(\frac{\partial v}{\partial z}\right)^2\right] \quad (7)$$

In equation (7), c,ρ and k are the specific heat, density and heat transfer coefficient of the lubricating oil, respectively; u and v are the flow velocities of lubricating oil along x and y directions. The expression of q is:

$$q=\frac{\partial}{\partial x}\int_0^z\rho u\mathrm{d}z'+\frac{\partial}{\partial y}\int_0^z\rho v\mathrm{d}z'$$

The energy equations of the two solids (Xu, 2011) are rewritten as:

$$\begin{cases}c_a\rho_a u_a\dfrac{\partial t}{\partial x}=k_a\left(\dfrac{\partial^2 t}{\partial z_a{}^2}+\dfrac{\partial^2 t}{\partial x^2}+\dfrac{\partial^2 t}{\partial y^2}\right)\\ c_b\rho_b u_b\dfrac{\partial t}{\partial x}=k_b\left(\dfrac{\partial^2 t}{\partial z_b{}^2}+\dfrac{\partial^2 t}{\partial x^2}+\dfrac{\partial^2 t}{\partial y^2}\right)\end{cases} \quad (8)$$

where $c_{a,b}$, $\rho_{a,b}$ and $k_{a,b}$ are specific heat, density and heat conductivity of surface a and b, respectively. As it is a finite length line contact problem, the heat conduction along x- and y-directions should also be involved.

The heat flux continuity conditions (Yang, 1998) on the two oil-solid interfaces are:

$$\begin{cases}k\dfrac{\partial t}{\partial z}\Big|_{z=0}=k_a\dfrac{\partial t}{\partial z_a}\Big|_{z_a=0}\\ k\dfrac{\partial t}{\partial z}\Big|_{z=k}=k_b\dfrac{\partial t}{\partial z_b}\Big|_{z_b=0}\end{cases} \quad (9)$$

The temperature boundary condition at the upstream of the oil film (Yang, 1998) is:

$$t(x_{\mathrm{in}},y,z)=t_0\quad\left(u(x_{\mathrm{in}},y,z)\geq 0\right) \quad (10)$$

The temperature boundary conditions for the bush and the pin are:

$$\begin{cases}t(x_{\mathrm{in}},y,z_a)=t_0,t(x_{\mathrm{in}},y,-d)=t_0\\ t(x_{\mathrm{in}},y,z_b)=t_0,t(x_{\mathrm{in}},y,d)=t_0\end{cases} \quad (11)$$

where, d is the depth of the variable temperature layer.

The load balance equation (Xu, 2011) reads:

$$\int_{-l}^{l}\int_{x_{\mathrm{in}}}^{x_{\mathrm{out}}}p\mathrm{d}x\mathrm{d}y=w \quad (12)$$

In equation (12), w is the load applied to contact area.

The Roelands viscosity-pressure-temperature relation (Yang, 1998) and the density-pressure-temperature relation (Yang, 1998) of the oil are also used.

2.2 Numerical techniques

Programming is carried out after non-dimensionalization of the governing equations. However, the results are given using dimensional forms. The several dimensionless parameters (Xu, 2011) involved are as follows: The dimensionless parameters:

$$W = w/(2E'rl),\ X = x/b,\ Y = y/b,$$

where, $b = r\sqrt{8W/\pi}$, $p_H = E'b/r$.

The oil film pressure is solved by a multigrid method (Venner and Lubrecht, 2000) and the elastic deformation is solved by a multi-level multi-integration technique (Venner and Lubrecht, 2000). Using a four-layer grid, the number of nodes is 128 in X-direction and 512 in Y-direction on the finest grid level. A line-line scanning method (Yang, 1998) is used to calculate the temperature field. As for the convergent criteria, the relative error of pressure is less than 10^{-3}, and the relative errors of temperature and load are less than 10^{-4}.

3. Results analysis

In the calculation, the ambient viscosity of the oil η_0 = 0.08 Pa·s, the viscosity-pressure coefficient α = 2.19×10^{-8} Pa^{-1}, the ambient temperature t_0 = 303 K, the bush and the pin form a steel-steel contact, so material parameter G = 5000. The contact surfaces are smooth and the lubricant is assumed as a Ree–Eyring fluid. The surface speeds are set as: u_a = 1 m/s, u_b = 0. The maximum Hertz pressure p_H = 0.2 GPa unless otherwise stated.

3.1 The influence of equivalent radius

Figure 3 shows the results by the change of the equivalent radius of curvature at the mid-sections in Y = 0 and X = 0 directions, respectively, from r = 0.03 m to 2 m, the corner radius at both ends of the bush r_{end} = 0.5 m, the generatrix length of the bush l_0 = 30 mm, the rounded length at both ends y_{sk} = 5 mm. In Figure 3, p, h, t are dimensional pressure, thickness and temperature of oil film, respectively. The temperature rise profiles are selected at the middle of the oil film in Z-direction.

Because of the stress concentration at the end of the bush, for the mid-section pressure at Y = 0, the increase of the equivalent radius of curvature plays a role like the decrease of the entraining velocity. For r = 0.03 m, there is only a pressure peak, with the increase of r, the pressure peak moves towards the outlet direction with a decreasing height. At r = 0.3 m, a pressure spike starts to appear. For r = 2 m, the pressure spike becomes lower and rounded. The decrease of the pressure peak is also seen in the middle of the pressure profiles along X = 0 section. Meanwhile, there are pressure spikes at both ends of the contact, forming an M-shape. With the increase of r, the height the spikes at both ends is continuously increasing. At r = 2 m, the height of the pressure spikes is 0.325 GPa, exceeding around 62.5 per cent of its maximum Hertzian contact p_H. Meanwhile, the central pressure is kept at around 0.2 GPa.

For the film thickness along Y = 0 section, it increases with the increase of r. While the outlet constriction becomes more and more obvious during the process. In the X = 0 section, with r = 0.03 m, the film thickness profile is horizontal with only two tiny lobes at both edges. For r = 0.1 m and 0.3 m, the film thickness is lifted as a whole, together with the two side lobes. For the rest 3 values of r, the central part is increased while the two side lobes gains size and drop continuously. The lowest point of the side lobes for r = 2 m is close to the level of those lobes for r = 0.03 m. The oil film shape at X = 0 section evolves form a U-shape to a W-shape with the increase of r.

The temperature rise at the Y = 0 section is not significant. For r = 0.03 m and 0.1 m, there shows only a temperature rise peak. The peak for r = 0.1 m is higher and closer to the exit than that of r = 0.03 m. A temperature spike occurs at r = 0.3 m, which moves towards the outlet with the increase of r. As for the temperature rise along X = 0 section, it resembles the variation of the corresponding pressure profile at X = 0 section. The central part is reduced slightly while the side spikes increases drastically with the increase of r. When r = 2 m, the maximum temperature reaches 50°C.

Figure 4 shows the variation of central film thickness, minimum film thickness, friction coefficient and maximum temperature rise of the oil film with the change of the equivalent radius of curvature r. As is seen from Figure 4, with the increase of r, the central film thickness increases continuously; the minimum film thickness increases a little first and then decreases, and eventually tends to be flat. The maximum temperature of the oil film increases linearly. The friction coefficient in the contact zone decreases sharply from r = 0.03 m ~ 0.2 m, followed by a gentle curve thereafter.

3.2 The influence of the bush length

Considering that chains with different numbers own different bush lengths, the influence of generatrix length of bush l_0 on the oil film is also explored, as shown in Figure 5. The input parameters are: r = 0. 3 m, r_{end} = 0.5 m, y_{sk} = 4 mm, l_0 are 8, 10, 12, 14, 16, 18 mm, respectively. To facilitate the comparison of the results, dimensionless coordinates in X-direction and dimensional coordinates in Y-direction are used. As can be seen from Figure 5, when l_0 is 8 mm, the pressure, film thickness and temperature rise in the contact zone resemble those in point contact. l_0 = 8 mm makes the contact area the smallest. Therefore, for the same applied load, the contact pressure, temperature rise in X = 0 and Y = 0 section are higher, while the film thickness is subsequently thinner. With the increase of l_0, the contact area is increased, so that the contact pressure as well as the temperature rise is gradually reduced, accompanying with increase of the film thickness. For both pressure and the temperature rise profiles in X = 0 section, from l_0 = 10 to 18 mm, the two side spikes developed become lower and lower in expanding process in the two directions. The film thickness at the corresponding position is lifted correspondingly.

4. Discussion

In Figure 3, it is seen that the dimensional film thickness along Y = 0 section increases with the increase of the equivalent radius of curvature r. Zhang *et al.* (2019) found that the dimensionless

Figure 3 Pressure, film thickness and temperature rise profiles along $Y = 0$ and $X = 0$ sections with increase of r(l_0 = 30 mm, r_{end} = 0.5 m, y_{sk} = 5 mm)

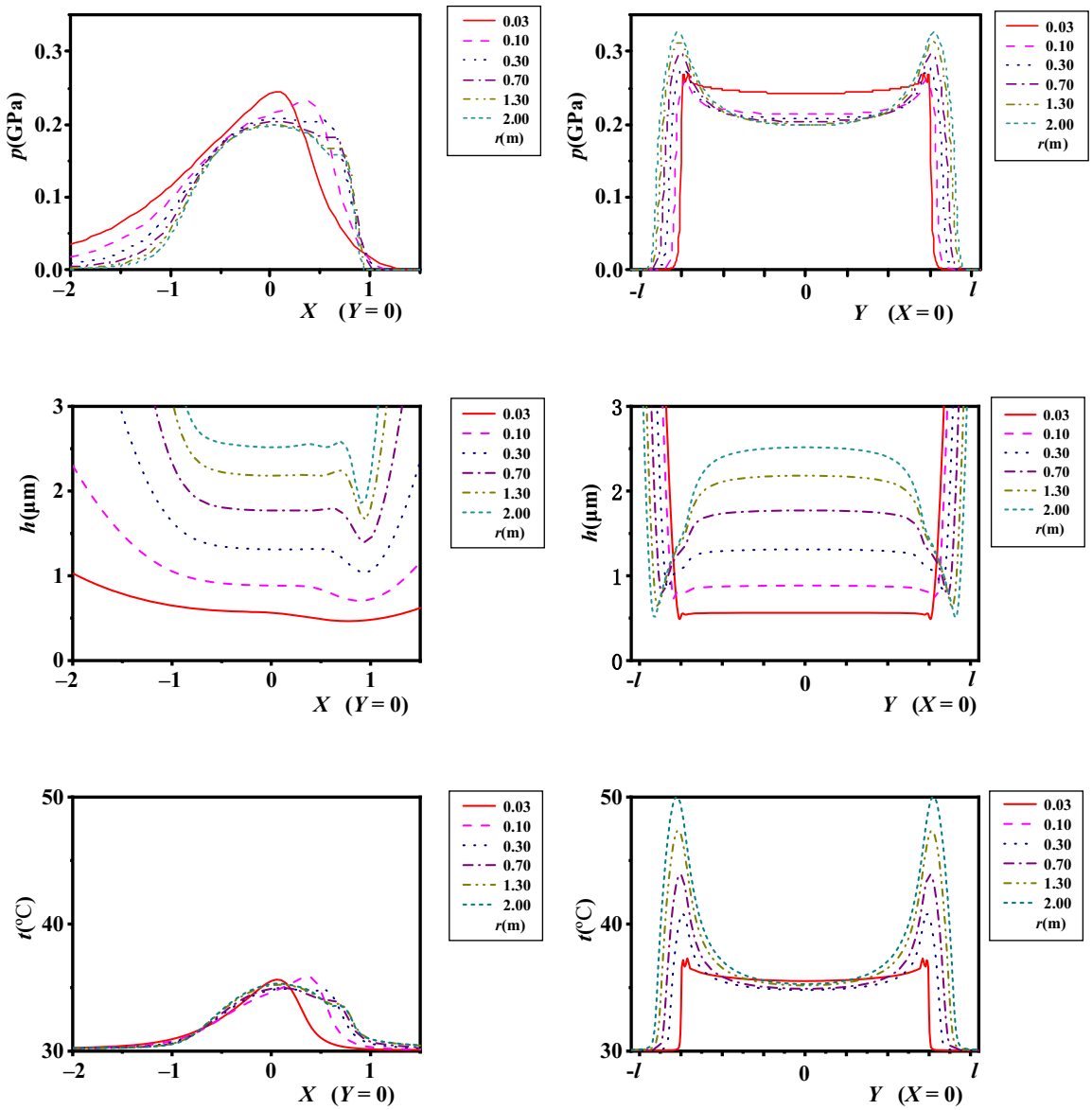

Figure 4 Changes of oil film thickness, friction coefficient and maximum temperature rise with the increase of equivalent radius r

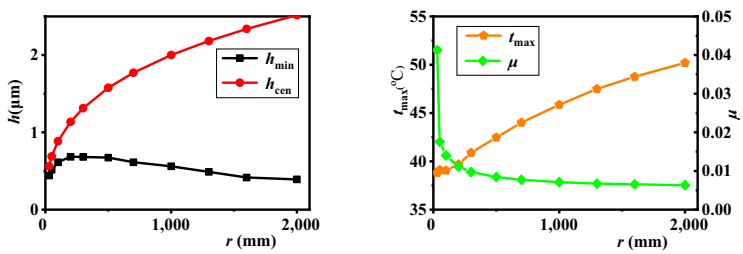

film thickness in infinite line contact decreased with the increase of the equivalent radius of curvature r. However, the variation (Zhang *et al.*, 2019) is the same as in Figure 3 if the dimensionless film thickness is changed into a dimensional form. For the finite line contact, the difference exists at the two edges of the contacts (at X = 0 section), the minimum film thickness firstly increases with the equivalent radius of curvature r and then decreases with further increase of r.

Figure 5 The influence of bush length on the oil pressure, film thickness and temperature rise profiles (r = 0.3 m, r_{end} = 0.5 m, y_{sk} = 4 mm)

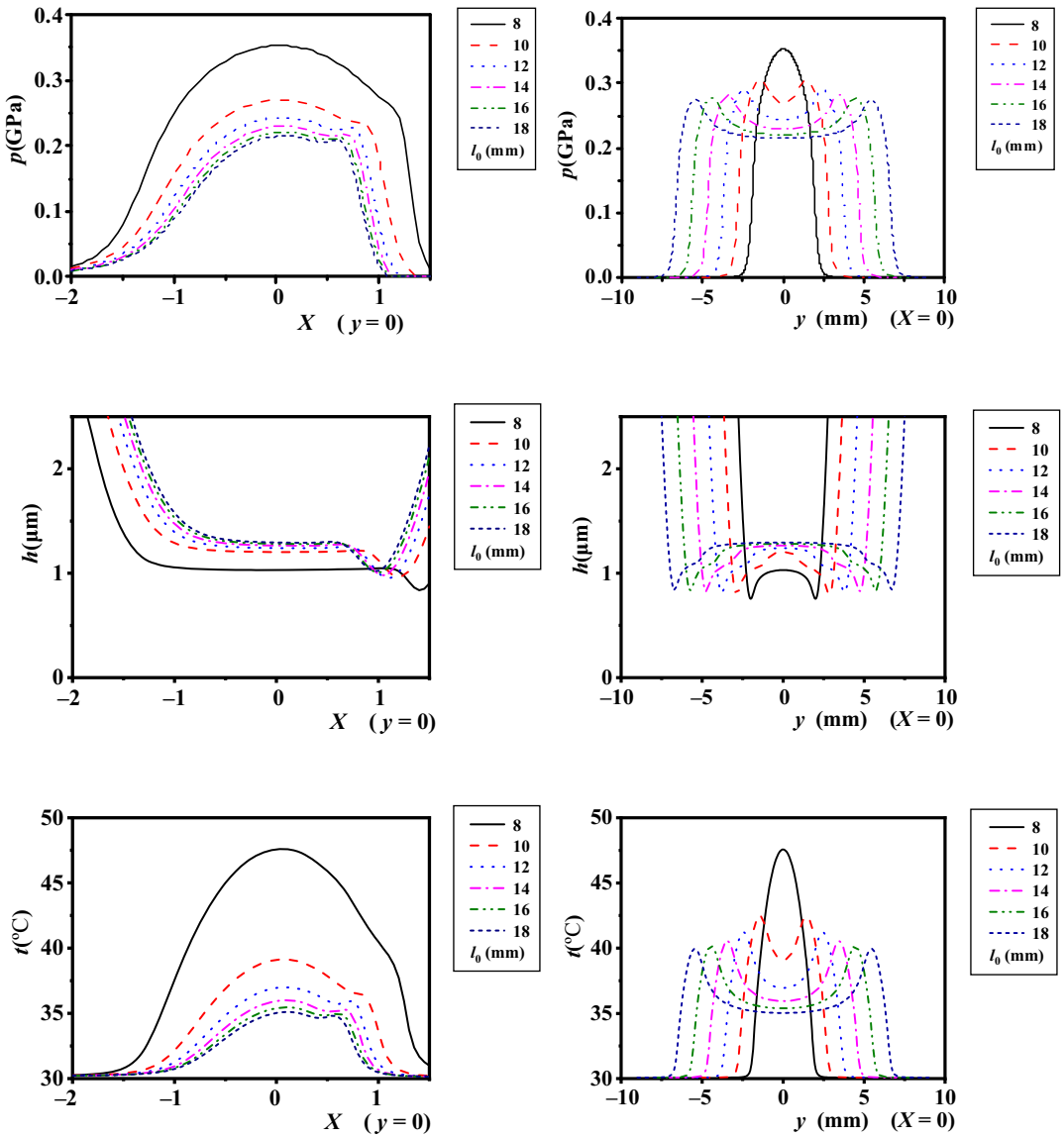

The contact between the bush and the pin is a transient problem. Not only the surface speed of the bush is transient, but also the applied load is changing with time. However, in the current work, the contact is assumed as a steady-state one with constant applied load. Nevertheless, the findings obtained will be helpful in understanding the the transient numerical results in the next step.

5. Conclusion

- Under specific working conditions, there exists an optimal equivalent radius to maximize the minimum oil film thickness in the contact zone.
- The increase of generatrix length l_0 will weaken the stress concentration effect in the rounded corner area at both ends of the bush, which can improve the wear resistance of chain.

References

Cheng, Y., An, L., Yin, S. and Wang, X. (2016), "Multi-variation characteristic of dual phase Hy-Vo silent chain transmission system", *Mechanism and Machine Theory*, Vol. 103 No. 9, pp. 40-50.

International standard iso 606 (1994), "Short pitch transmission precision roller chains and chain wheels", GB/T 1243-1997.

Liu, X.L., Cui, J.L. and Yang, P.R. (2012), "Size effect on the behavior of thermal elastohydrodynamic lubrication of roller pairs", *Journal of Tribology*, Vol. 134 No. 1, p. 11502.

Meng, F.Z., Zhao, F. and Lu, B.M. (2000), "Study on wear characteristics of timing chain and transmission chain of motor cycle", *Tribology*, Vol. 20 No. 4, pp. 106-109.

Mihailidis, A., Agouridas, K. and Panagiotidis, K. (2013), "Non-Newtonian starved thermal-elastohydrodynamic

lubrication of finite line contacts", *Tribology Transactions*, Vol. 56 No. 1, pp. 88-100.

Peeken, H. and Coenen, W. (1986), "Influence of oil viscosity and various additives on the wear of roller chains", *Wear*, Vol. 108 No. 4, pp. 303-321.

Ren, N., Zhu, D., Chen, W.W., Liu, Y. and Jane Wang, Q. (2009), "A three-dimensional deterministic model for rough surface line-contact EHL problems", *Journal of Tribology*, Vol. 131 No. 1, p. 11501.

Rosenkranz, A., Krupp, F., Reinert, L., Mücklich, F. and Sauer, B. (2017), "Tribological performance of laser-patterned chain links-influence of pattern geometry and periodicity", *Wear*, Vols 370/371 No. 1, pp. 51-58.

Venner, C.H. and Lubrecht, A.A. (2000), *Multilevel Methods in Lubrication*, Elsevier, Amsterdam.

Xu, H. (2011), "Analyses of the thermal hydrodynamic lubrication of the oil film between elastic rollers", Master Thesis, Qingdao University of Technology.

Xu, X.Q., Zhao, J.X. and Meng, F.Z. (2017), "Study on the wear-resisting performance of automobile engine timing bush chain", *Journal of Mechanical Transmission*, Vol. 41 No. 12, pp. 106-107.

Yang, P. (1998), *Numerical Analysis of Fluid Lubrication*, National Defense Industry Press, Beijing.

Zhang, M.Y., Wang, J., Liu, Y., Dai, L.J. and Shang, Z.H. (2019), "Size effect on thermal elastohydrodynamic lubrication of industrial chain bush-pin hinge pair", *Industrial Lubrication and Tribology*, Vol. 71 No. 9, doi: 10.1108/ILT-10-2018-0369.

Zhu, D., Wang, J., Ren, N., J. and Wang, Q. (2012), "Mixed elastohydrodynamic lubrication in finite roller contacts involving realistic geometry and surface roughness", *Journal of Tribology*, Vol. 134 No. 1, p. 11504.

Corresponding author

Jing Wang can be contacted at: wj20011226@163.com